LANGMUIR

pubs.acs.org/Langmuir Article

Metal–Organic Framework UiO-66-Mediated Dual-Signal Ratiometric Electrochemical Sensor for microRNA Detection with DNA Walker Amplification

Fa-Ting Xie, Yu-Long Li, Tong Yang, Yun-Hui Yang,* and Rong Hu*

Cite This: *Langmuir* 2022, 38, 11828–11836 Read Online

ACCESS | Metrics & More | Article Recommendations | Supporting Information

ABSTRACT: Electrochemical nanotags with strong signal input are necessary for a ratiometric electrochemical sensor to overcome the drawbacks of inaccurate detection results. In this paper, the metal–organic framework (MOF) UiO-66 was utilized as an electrochemical signal tag. A stable and strong current response at +0.9 V can be detected in neutral conditions. MicroRNA (miRNA) was employed as the model analyte. Herein, an enzyme-free DNA-walker-based ultrasensitive ratiometric electrochemical biosensor in combination with Zr MOF (UiO-66) signal tags to detect miRNA was demonstrated. In the presence of miRNA, the autonomous walker movement can be initiated by miRNA, leading to the release of biotin-modified fragments. Thus, streptavidin-labeled UiO-66 nanomaterials were not bound to the electrode, generating a low signal response of UiO-66 at +0.9 V. However, the current signal of electrolyte solution as reference at +0.2 V was increased due to the enhancement of electrode conductivity. This ratiometic sensor demonstrated high sensitivity, selectivity, and reproducibility. It can eliminate the disturbance of environmental factors and basic electrode characteristics, providing more accurate signals. A limit of detection (LOD) of 0.17 fM was achieved. Moreover, the method was also used to detect miRNA-21 spiked in real serum samples.

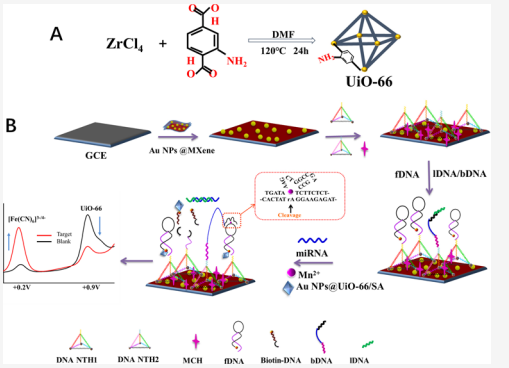

INTRODUCTION

Electrochemical methods, especially the ratiometric biosensor, with low cost, high selectivity and sensitivity, and high reproducibility, and portability, have emerged as attractive techniques for detecting clinical samples.[1−3] Instrumental efficiency and environmental factors can affect a biosensor's reproducibility. With built-in correction, ratiometric biosensors can be provided with a more stable response based on the sensor's self-referencing capabilities.[4−6] Distinguishable signal tags are an important factor for electrochemical biosensors. With traditional electroactive organic substances (e.g., methylene blue (MB) and thionine, ferrocene), their electrochemical signals are usually decreased when they conjugated to the recognition elements (e.g., DNA, antibody), leading to unstable results and poor repeatability. Electroactive nanomaterials with tunable electrochemical signals by changing their composition and structures including quantum dots and metal nanoparticles have also been widely used.[7−9] They can greatly amplify the signal in the sensing system. However, their electrochemical signals are usually generated under strong acid or alkali conditions.

Metal–organic frameworks (MOFs) are an ordered network structure, which are assembled by organic bridging ligands and metal ions.[10−14] In particular, Zr MOFs with permanent porosity and high chemical stability are promising candidates for biosensors and therapy.[15−17] Tan and co-workers demonstrated that nanoscale Zr MOF nanoparticles could be used as quenchers for bioimaging purposes and photodynamic therapy.[15] Qu et al. synthesized N-propyl-4-hydrazine-naphthalimide-modified MOFs for the detection of formaldehyde.[16] Recently, UiO-66 was used as a signal tag in electrochemical biosensors. For instance, Chang et al. reported a porous UiO-66 loaded with electroactive dyes, which was applied to detect microRNA.[18] Lei et al. reported a DNA-walker-triggered conformation switch in combination with a MOF that was developed as a tag for DNA analysis.[19] Meanwhile, detection in strong alkaline conditions (pH 11) with $NaBH_4$ might affect the DNA binding because of the liberation of some DNAs from the electrode. The leakage of dye from MOFs might be a potential problem. In this paper, we find that UiO-66 itself could be used for signal tags, which can be detected in neutral conditions. Pretreatment, acid dissolution, and $NaBH_4$ were not required. Noble metal particles can easily be incorporated inside the UiO-66 shell, improving the stability of MOFs. The

Received: April 11, 2022
Revised: September 7, 2022
Published: September 23, 2022

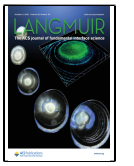

https://doi.org/10.1021/acs.langmuir.2c00932
Langmuir 2022, 38, 11828–11836

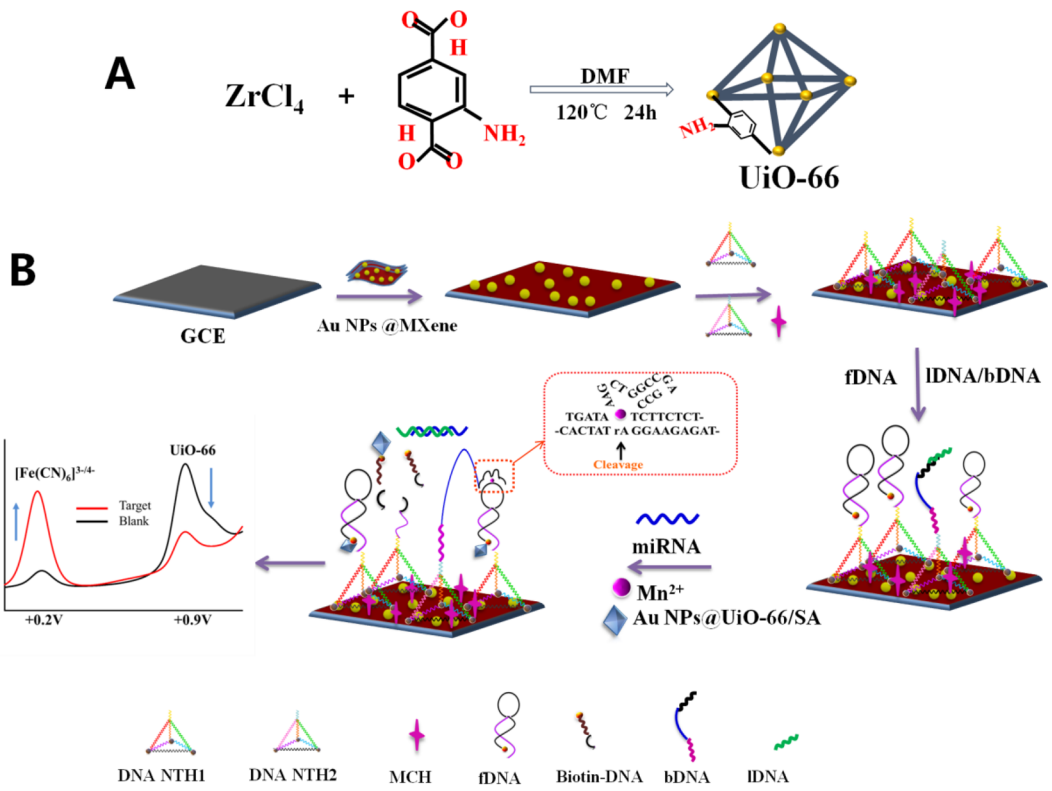

Figure 1. (A) Schematic preparation of UiO-66 nanomaterial. (B) Principle of the ratiometric electrochemical biosensor.

electroactive tag UiO-66 with a stable and high signal is desirable for a electrochemical biosensor.

A tumor biomarker, such as microRNA (miRNA) and a microvesicle, is one of the most reliable methods for early tumor screening, since they are abnormally produced/elevated by the body's response to tumors.[20,21] Studies have shown that miRNA can regulate many cellular processes, such as development, proliferation, and apoptosis.[22,23] Alterative expressions of miRNAs can result in various human diseases such as an altered immune system and cancer.[24−26] However, the concentration of miRNAs is low (≤pM) in biological samples, such as serum. An amplification method is necessary for analyzing miRNAs.

DNA walker movement autonomously along the track could amplify the signals.[27,28] In the past few decades, DNA walkers have gained widespread attention and have been widely utilized for biosensor and diagnostic system application. For instance, Zou et al. reported enzyme-assisted DNA walkers for the detection of ctDNAs.[29] Zhu et al. demonstrated a tripedal DNA walker based on target-induced hairpin assembly for miRNA analysis.[30] In contrast to enzyme-based DNA walkers, owing to being inexpensive and easy to build, enzyme-free DNA walkers were identified as a more beneficial strategy, especially for DNA tetrahedral nanostructure (NTH)-based enzyme-free DNA walkers. NTH bound to the electrode surface can control the orientation of a probe and reduce local overcrowding effects.[31−33] These characteristics could enhance the efficient DNA walkers to improve the sensitivity of sensors.

Herein, we demonstrate an enzyme-free DNA-walker-based ratiometric electrochemical biosensor in combination with Zr MOF (UiO-66) signal tags to detect miRNA (Figure 1). We use miRNA as a model analyte. The walker movement can be initiated in the presence of miRNA, leading to the release of biotin-modified fragments. Upon the addition of UiO-66/streptavidin nanomaterials (UiO-66/SA, signal probe, SP), a small number of Zr MOFs could bind to the electrode, and low current intensity at +0.9 V could be detected. However, the current signal of electrolyte solution $K_3Fe(CN)_4/K_4Fe(CN)_6$ as an inner reference probe (IR) at +0.2 V can be increased. Therefore, a ratiometric electrochemical strategy based on UiO-66 MOF and $K_3Fe(CN)_4/K_4Fe(CN)_6$ was constructed, providing more accurate signals in which environmental factors and basic electrode characteristics were eliminated. And UiO-66/SA complexes were not required to covalently cross-link with nucleic acid, simplifying the sensor's procedure. Compared with commercial tags of methylene blue, the signal of UiO-66 was much stronger than that of MB. As expected, using the Zr MOF signal tags to obtain strong signals, with NTH-based-DNA walker signal amplification, the proposed method showed ultrasensitivity to miRNA-21 with a limit of detection of 0.17 fM. Our proposed method is expected to be applied in early disease diagnosis and clinical biomedicine.

EXPERIMENTAL SECTION

Materials and Apparatus. Zirconium(IV) chloride, 2-amino-terephthalic acid, streptavidin (SA), and $HAuCl_4$ were purchased from Sigma-Aldrich Inc. Ascorbic acid (AA), urea, dopamine (DA), glutathione (GSH), glycine (Gly), tryptophan (Trp), bovine serum albumin (BSA), L-threonine (L-thr), and L-cysteine (L-Cys) were purchased from Aladdin Biochemical Technology Co., Ltd. (Shanghai, China). MXene was received from Forsman Technology Beijing Co., Ltd. (Beijing, China). DNA sequences were supplied by Sangon Biotech Co., Ltd. (Shanghai, China). The sequences are shown in Table S1.

All electrochemical measurements were measured with a three-electrode system by a CHI 660D Chenhua electrochemical workstation (Shanghai, China). A glassy carbon electrode (GCE, d = 3 mm) was utilized as the working electrode. A platinum wire was used

https://doi.org/10.1021/acs.langmuir.2c00932
Langmuir 2022, 38, 11828−11836

as the auxiliary electrode, and Hg/HgCl (saturated KCl) was employed as the reference electrode.

Synthesis of DNA NTH Material. DNA NTH was synthesized via a previously reported method.[34] The synthesized concentration of DNA NTH 1 was 1.75 μM. The concentration of DNA NTH 2 was 0.87 μM.

Preparation of Gold Nanoparticles@UiO-66 (Au NPs@UiO-66). Au NPs were synthesized by the reported literature.[35] Briefly, 50 mL of water and 500 μL of $HAuCl_4$ (1 wt %) were placed in a reaction vessel. The mixture was heated with constant stirring until reflux. After boiling, 1 w% of 1.75 mL of trisodium citrate liquid was added dropwise, and heating was stopped until the liquid turned wine red. The mixture was then cooled and placed in an airtight environment at 5 °C.

UiO-66 was prepared via the literature with some modification.[36] Zirconium(IV) chloride (0.0543 g, 0.233 mM) and 2-amino-terephthalic acid (0.0422 g, 0.233 mM) were mixed in 3 mL of DMF. After ultrasonic treatment for half an hour, the mixture was moved to an autoclave for 24 h at 120 °C. Then, the reaction mixture was cooled and heated in DMF at 60 °C for 1 day. Next, the precipitate was centrifuged (6000 r/min), washed 3 times with DMF and alcohol, and dried at 65 °C.

Then, 30 mL of Au NP solution was added slowly to 30 mL of UiO-66 solution (0.5 mg/mL) and continuously stirred for a day. After centrifugation (5000 r/min), the product was washed several times with water to remove excess Au NPs. Then, the precipitate was dried in a vacuum oven at 65 °C to obtain the Au NPs@UiO-66.

Synthesis of Au NPs@MXene. MXene (20 mg) was added to 50 mL of water. Then, the MXene was ultrasonicated until well-dispersed, and 600 μL of 100 mM $HAuCl_4$ was slowly added with continuous stirring for 10 min. The resulting Au NPs@MXene mixture was centrifuged at 5000 r/min. Finally, the collected precipitates were dried in a vacuum drying oven at 60 °C.

Synthesis of Au NPs@UiO-66/Streptavidin (Au NPs@UiO-66/SA) Hybrids. Au NPs@UiO-66 (10 mg) was dispersed in 500 μL of water. To the above suspension, 200 μL of 1-(3-(dimethylamino)-propyl)-3-ethylcarbodiimide hydrochloride (400 mM) and 200 μL of *N*-hydroxysuccinimide (100 mM) were added and reacted for half an hour. After centrifugation and washing with buffer (0.025 M PBS, pH 7.4), 200 μL of streptavidin (500 μg/L) was added at 5 °C and kept for 3 h. Finally, the reaction mixture was centrifuged (6000 r/min) and rinsed with buffer for three times. The precipitates were added to 500 μL of buffer and stored at 5 °C.

Sensor Preparation and Detection Method. First, 10 μL of a Au NPs@MXene dispersion with 10 μL of chitosan solution was added to a clean electrode and dried. Afterward, 20 μL of synthesized DNA NTH1 and NTH2 was added to the modified GCE electrode for overnight, followed by dropping 10 μL of MCH solution and incubating at 25 °C for 10 min to lock the remaining sites. Immediately, 10 μL of the lDNA/bDNA and fDNA mixture was dropped to the modified GCE for 1.5 h at 25 °C. Then, 5 μL of 6 mM $MnCl_2$ solution was added on the GCE for 15 min. After that, the GCE was modified by adding 5 μL of miRNA-21, followed by 1.5 h of incubation. Finally, 10 μL of Au NPs@UiO-66/SA hybrids was coated on the GCE for 90 min at 25 °C. After each step, the GCE was washed with PBS buffer to prepare for the next step. The electrochemical measurement was performed from 0.05 to 1.15 V in 20 mM Tris-HCl buffer (pH 7.4) containing 200 mM $[Fe(CN)_6]^{3-/4-}$ by using a differential pulse voltammetric (DPV) method for quantitative detection of miRNA-21.

RESULTS AND DISCUSSION

Design Strategy. In order to realize the quantitative detection of miRNA-21, the principle of the proposed electrochemical ratiometric sensing system is represented in Figure 1. DNAzyme, specific to manganese ions, is utilized to construct an enzyme-free DNA walker, which provides energy through DNAzyme-mediated catalytic and hydrolytic activities toward specific substrates. Traditional ratiometric electrochemical biosensors usually label two signal tags on a nucleic acid or antibody. One is for the signal probe, and another is for the reference probe. These modifications increase the cost of a biosensor. Furthermore, the labeling might fail even if it is purchased from a commercial company. Electrolyte solutions, such as $K_3Fe(CN)_4/K_4Fe(CN)_6$ and toluidine blue, can be a good replacement for the reference probe, since they are cheap, stable, and can be used without modification. First, the GCE electrode was decorated with Au NPs@MXene. Two types of thiol (HS)-labeled DNA NTHs were attached to the GCE via the Au−S bonds. Thus, two DNA strands named fDNA and bDNA were bound to the ends of the DNA NTH to become DNA walker substrates. The biotin-labeled fDNA is a hairpin structure containing a loop with the sequence of the substrate for DNAzyme. The swing DNA (bDNA) incorporates a DNAzyme sequence. In the absence of miRNA-21, DNAzyme was silenced through the locking DNA strand (lDNA). Upon addition of target, lDNA was removed by the toehold strand displacement to formation of miRNA-21/lDNA double-stranded DNA. Thus, DNAzyme in swing DNA can be activated. Afterward, the walker movement can be worked by cleavage of the activated DNAzyme toward fDNA upon addition of Mn^{2+}. These operations are self-powered without the external energy supply. In addition, a DNA walker with autonomous movement triggers the successive release of biotin-labeled nucleotide fragments from the fDNA. After the addition of SA-labeled UiO-66, a low DPV signal response at +0.9 V was detected. DNA is a nonconductive material. When part of the DNA falls off the surface of the electrode, it results in relatively high conductivity of the modified electrode. Therefore, a high DPV signal response was obtained for $K_3Fe(CN)_4/K_4Fe(CN)_6$ at +0.2 V. Accordingly, miRNA-21 concentrations could be monitored according to the ratio responses ($I_{[Fe(CN)6]^{3-/4-}\text{-IR}}/I_{\text{UiO-66-SP}}$).

In order to verify the rationality of this experiment, control experiments under different conditions were conducted. The electrochemical responses to different detection conditions are displayed in Figure 2A. As depicted in Figure 2A, only the fDNA strand has a low $I_{[Fe(CN)6]^{3-/4-}\text{-IR}}/I_{\text{UiO-66-SP}}$ signal. A large amount of UiO-66 links with fDNA on the electrode, resulting in a strong current signal at +0.9 V. Moreover, fDNA is a nonconductive material that hinders the transfer of electrons, so a low response of $[Fe(CN)_6]^{3-/4-}$ was detected for an electrode. After introduction of miRNA (1 pM), miRNA can hybridize with lDNA, and DNAzyme in swing bDNA can be activated. When fDNA and bDNA containing DNAzyme were mixed when Mn^{2+} was not added, the $I_{[Fe(CN)6]^{3-/4-}\text{-IR}}/I_{\text{UiO-66-SP}}$ ratio value obtained was similar to that of the fDNA strand. After 6 mM Mn^{2+} was added to the mixture, 9-fold electrochemical signal enhancement was obtained. It was attributed to the DNAzyme catalyzing the cleavage of substrate (fDNA), dissociating a particular base pair in the fDNA. Biotin-labeled DNA fragments in fDNA departed from the electrode. Consequently, SA-labeled UiO-66 cannot bind with them. Therefore, a high $I_{[Fe(CN)6]^{3-/4-}\text{-IR}}/I_{\text{UiO-66-SP}}$ value was detected. Moreover, only a bDNA strand or bDNA/lDNA complexes have a high $I_{[Fe(CN)6]^{3-/4-}\text{-IR}}/I_{\text{UiO-66-SP}}$ value (Figure S1), since only the response of $[Fe(CN)_6]^{3-/4-}$ can be detected. The obtained dates confirmed the feasibility of our strategy.

Characterization. A DNA tetrahedron is formed by the end-to-end ligation of four DNA sequences (Tetra Mn and Tetra Mn B−D). The DNA tetrahedron was first confirmed by

https://doi.org/10.1021/acs.langmuir.2c00932
Langmuir 2022, 38, 11828−11836

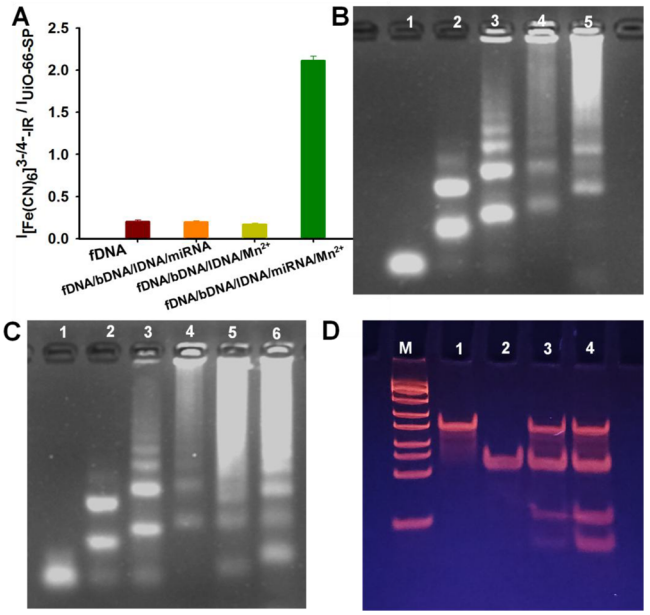

Figure 2. (A) Feasibility of our experiment. Gel electrophoresis images: (B) (1) Tetra-Mn1, (2) Tetra-Mn1/Tetra-Mn1B, (3) Tetra-Mn1/Tetra-Mn1B/Tetra-Mn1C, (4) Tetra-Mn1B/Tetra-Mn1C/Tetra-Mn1D/Tetra-Mn1 (DNA NTH1), (5) Tetra-Mn1B/Tetra-Mn1C/Tetra-Mn1D/Tetra-Mn1/fDNA. (C) (1) Tetra-Mn2, (2) Tetra-Mn2/Tetra-Mn2B, (3) Tetra-Mn2/Tetra-Mn2B/Tetra-Mn2C, (4) Tetra-Mn2B/Tetra-Mn2C/Tetra-Mn2D/Tetra-Mn2 (DNA NTH2), (5) Tetra-Mn2B/Tetra-Mn2C/Tetra-Mn2D/Tetra-Mn2/bDNA, (6) Tetra-Mn2B/Tetra-Mn2C/Tetra-Mn2D/Tetra-Mn2/bDNA/lDNA. (D) Polyacrylamide gel electrophoresis (PAGE) result. (M) marker, (1) fDNA, (2) bDNA, (3) fDNA+ bDNA without Mn^{2+}, (4) fDNA+ bDNA with Mn^{2+}.

PAGE electrophoresis. As exhibited in Figure 2B, line 1 was Tetra Mn1. Lines 2 and 3 were loaded with Tetra-Mn1/Tetra-Mn1B and Tetra-Mn1/Tetra-Mn1B/Tetra-Mn1C, respectively. The movement was gradually slow with the increase of molecular weight (line 4), which demonstrated the successful synthesis of DNA NTH1 nanomaterials. The bands in track 5 indicated that fDNA was able to hybridize with tetrahedral DNA1. Figure 2C demonstrated the formation of DNA NTH2. The lines 1−3 were the same with DNA NTH1 (Figure 2B). Higher molecular weight and more steric complexity result in lower mobility for band 4 than previous bands (band 1−3). After the introduction of bDNA, the movement ran slower than that of DNA NTH2 (line 5). And lDNA can hybridize with tetrahedral bDNA (line 6). Polyacrylamide (PAGE) gel electrophoresis was also conducted. As shown in Figure 2D, fDNA or bDNA displayed low movement (lines 1 and 2). In the coexistence of fDNA, bDNA, and Mn^{2+}, a walker movement is triggered. A new, faster migrating band appears from the cleavage product of fDNA (line 4).

The successful synthesis of UiO-66 was first investigated using XRD. As evident from Figure 3A, the XRD patterns of the synthesized UiO-66 were highly coincident with previous reports,[36] suggesting its successful preparation. The Fourier transform infrared (FTIR) spectrum of prepared UiO-66 also matched with the literature (Figure 3B).[37] The peaks occurring at 3470 and 3382 cm^{-1} were the peaks of primary amines. The peak at 1255 cm^{-1} originates from the C−N bond. The morphology was observed using transmission electron microscopy (TEM). As depicted in Figure 3C, the freshly prepared UiO-66 nanomaterial had an irregular octahedral structure.[31] Moreover, gold nanoparticles were successfully adsorbed on the surface of UiO-66 (Figure 3D).

XPS analysis of Au NPs@UiO-66 was illustrated in Figure 3E−I. These dates displayed the presence of O, N, Au, Zr, and C components, indicating the formation of a Au NPs@UiO-66 complex (Figure 3E). In order to study the chemical state clearly, the spectrum of C 1s can be convoluted into two peaks at 285.8 and 289.5 eV, ascribed to −COO− and C−C groups, respectively (Figure 3F). Two symmetrical components could be fit into the N 1s spectrum (Figure 3G), which correspond to N−C[38] (399.4 eV) and N−H[39] (400.7 eV) functional groups. The Zr XPS spectrum can be convoluted into two peaks, as displayed in Figure 3H. These peaks occurring in 181.9 and 184.8 eV are consistent with Zr 3d and Zr 2p.[36] The Au spectrum of the Au NPs@UiO-66 can be divided into two symmetrical peaks situated at 84 and 87.8 eV that are consistent with Au 4f7 and Au 4f5 (Figure 3I), respectively, indicating that the surface of UiO-66 was successfully modified by Au NPs.

Figure 4A displays the XRD data of the synthesized MXene and Au NPs@MXene. The XRD analysis suggests that the crystal structures of MXene are quite similar to the previously reported structures (curve a).[40] The XRD analysis of the fabricated Au NPs@MXene further proved the formation of cubic Au (curve b).[40] And compared with bare GCE, the conductivity of Au NPs@MXene was 10-fold higher than that of GCE (Figure 4B). This property is very important for our proposed ratiometic electrochemical sensor, since the current signal of $[Fe(CN)_6]^{3-/4-}$ relies on the conductivity of the modified GCE. TEM was then utilized to investigate the morphologies of MXene and Au NPs@MXene. The TEM image of MXene nanosheets shows a two-dimensional wrinkled sheet structure (Figure 4C). Moreover, gold nanoparticles loaded on MXene nanosheets could also be observed in Figure 4D, indicating that the Au NPs@MXene composite was successfully synthesized.

Electrochemical Characterization of Biosensor Fabrication. The step-by-step construction process of our proposed biosensor was investigated in $[Fe(CN)_6]^{3-/4-}$ solution by electrochemical impedance spectroscopy (EIS) and cyclic voltammetry (CV). From Figure 5A, the bare GCE exhibited a small semicircle (Ret = 200 Ω) (curve a). Compared to bare GCE (curve a), the electrode coated with Au NPs@MXene exhibited a smaller semicircle (Ret = 90 Ω) (curve b), demonstrating that Au NPs@MXene enhances the electron transfer. When DNA nanotetrahedra were modified onto Au NPs@MXene-modified GCE, the Ret was enhanced to 640 Ω (curve c), which was triggered by the steric-hindrance effect on electronic transfer. Immobilized MCH blocked the redundant sites; therefore, in curve d, the Ret was increased to 850 Ω. Further, upon incubating lDNA + bDNA + fDNA, in curve e, the semicircle diameter was further increased (Ret = 2100 Ω). When miRNA-21 binds to lDNA, this results in the release of lDNA. The diameter of the semicircle decreased, and the Ret value was decreased to 1600 Ω (curve f).

Figure 5B shows the cyclic voltammetry curves for each phase of the sensor. As depicted in Figure 5B, the redox peaks corresponding to bare GCE were detected (curve a). The redox peaks were increased upon modification with Au NPs@MXene because it could enhance the electron transfer (curve

https://doi.org/10.1021/acs.langmuir.2c00932
Langmuir 2022, 38, 11828−11836

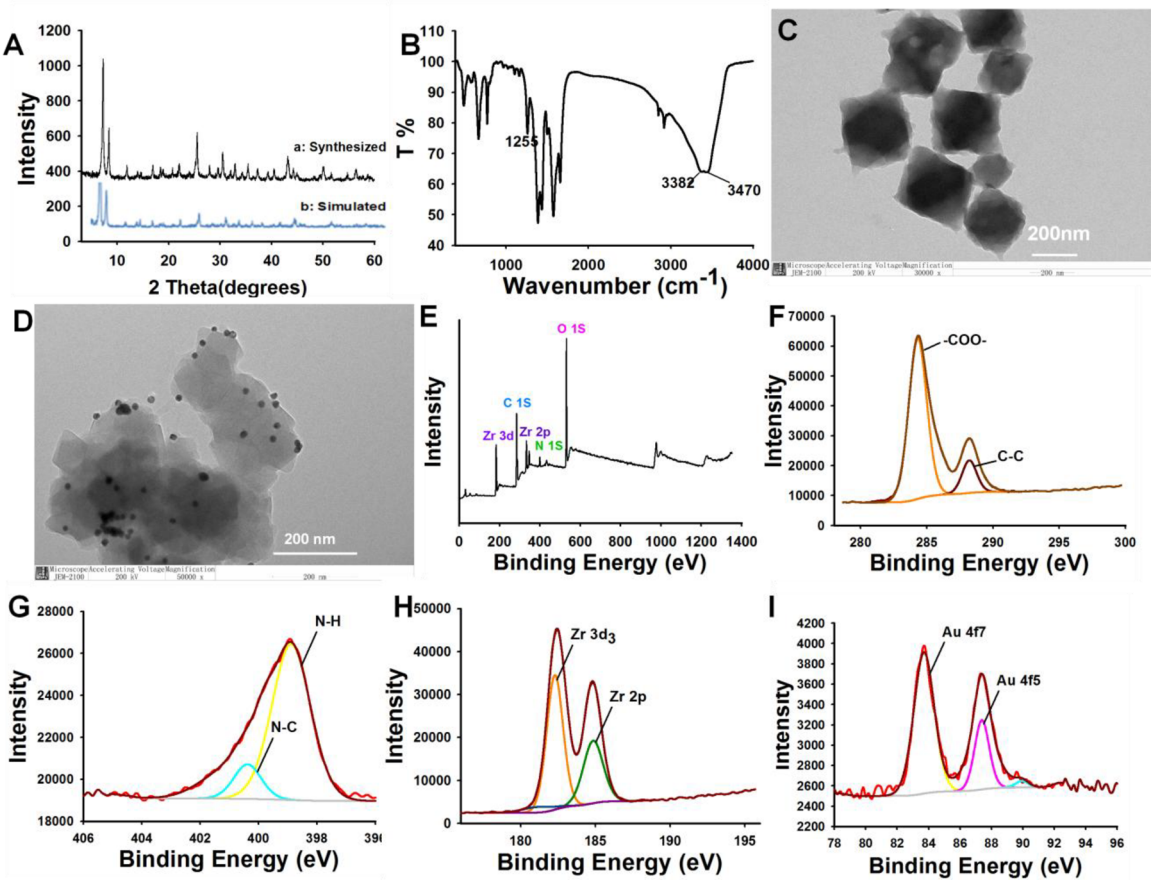

Figure 3. (A) XRD of UiO-66; (B) FTIR of UiO-66; (C,D) TEM images of UiO-66 and Au NPs@UiO-66; (E–I) XPS of Au NPs@UiO-66.

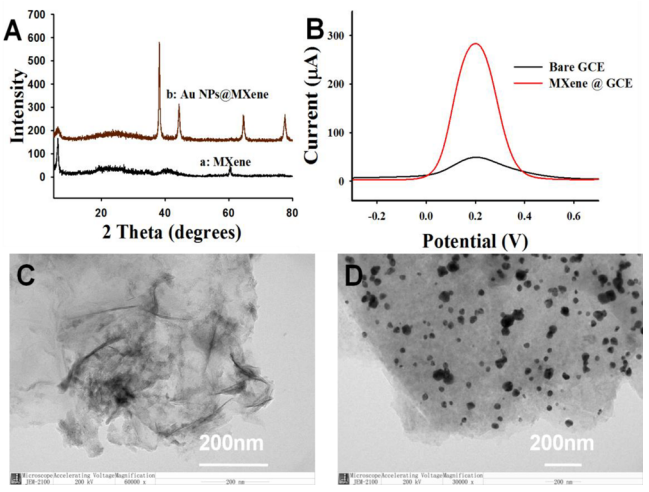

Figure 4. (A) XRD of MXene and Au NPs@MXene; (B) conductivity of Au NPs@MXene and bare GCE; TEM images of MXene (C) and Au NPs@MXene (D).

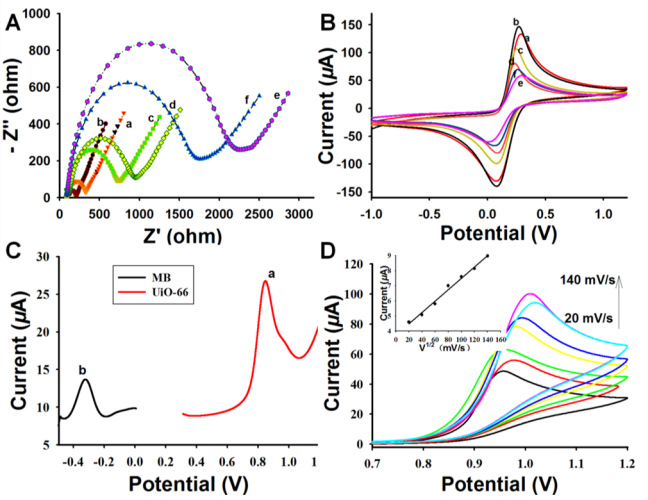

Figure 5. (A,B) EIS and CV of different modified GCEs in 5 mM $[Fe(CN)_6]^{3-/4-}$ containing 200 mM KCl ((a) bare GCE; (b) Au NPs@MXene/GCE; (c) DNA NTH/Au NPs@MXene/GCE; (d) MCH/DNA NTH/Au NPs@MXene/GCE; (e) lDNA+bDNA +fDNA/MCH/DNA NTH/Au NPs@MXene/GCE; (f) miRNA-21/lDNA+bDNA+fDNA/MCH/DNA NTH/Au NPs@MXene/GCE). Initial potential (V): 0.155; high frequency (Hz): 100 000; low frequency (Hz): 0.1; amplitude (V): 0.005; quiet times (s): 2. (C) DPV current response of (a) UiO-66 and (b) MB. (D) Cyclic voltammetry of UiO-66-modified GCEs with different scan rates; inset is the relationship between I_p and $v^{1/2}$.

b). After modification of DNA nanotetrahedra on GCE, the redox peaks decreased (curve c), owing to electrostatic repulsion. Next, the redundant sites were blocked with MCH, which greatly reduced the redox peak current (curve d). The redox peak current of MCH/DNA NTH/Au NPs@MXene/GCE was further decreased after incubation with the lDNA + bDNA + fDNA (curve e). And it was increased again after incubation miRNA-21 on the electrode (curve f).

https://doi.org/10.1021/acs.langmuir.2c00932
Langmuir 2022, 38, 11828–11836

We compare the current signal of methylene-blue-labeled fDNA with our SA-labeled MOFs. One can see in Figure 5C, the signal intensity of SA-labeled MOFs at +0.9 V (curve a) is much higher than that of methylene blue at −0.32 V (curve b). The strong electrochemical signal is very important for a highly stable and repeatability sensing system. At the same time, cyclic voltammetry of UiO-66 decorated GCEs at different potential scan rates (v) was then studied. One can see in Figure 5D, the current intensities were enhanced over the scan rate ranging from 20 to 140 mV/s. The inset is the linear relationship between peak current (I_p) with the square root of scanning rate ($v^{1/2}$). The Randle-Sevcik equation is $I_p = 2.69 \times 10^6 n^{2/3} A D^{1/2} C v^{1/2}$. The peak current is proportional to $v^{1/2}$, indicating that the current of UiO-66 is a diffusion-controlled process.

Optimization of the Experimental Conditions. In order to achieve the best performance, the effect of pH of buffer, Mn^{2+} incubation time, and concentration of Mn^{2+} were optimized to achieve higher sensitivity during the experiment. As presented in Figure 6A, the current value was increased

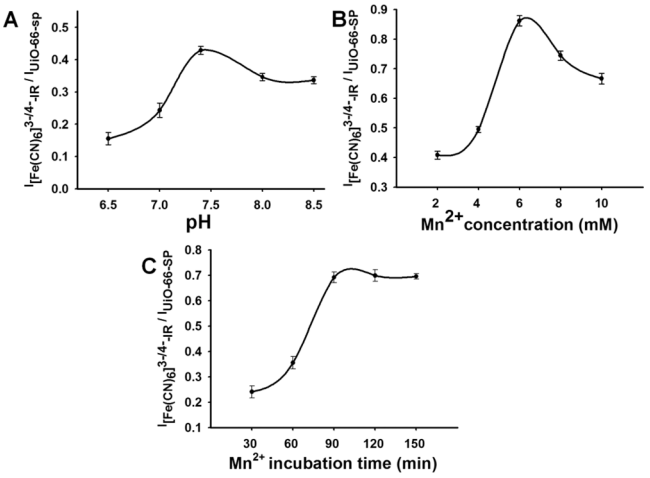

Figure 6. Effect of (A) pH, (B) concentration of Mn^{2+}, and (C) incubation time of Mn^{2+} on the response of sensing system.

with the enhancement of pH, and the maximum ratio value was obtained at pH of 7.4. The concentration of Mn^{2+} also has a significant effect on the sensitivity of the as-designed sensor. In Figure 6B, the current ratio value increased with successive enhancement in the concentration of Mn^{2+} from 2 to 6 mM and reached its maximum at 6 mM. Moreover, the current value does not change appreciably when the incubation time of Mn^{2+} is 90 min (Figure 6C). Hence, a pH of 7.4, 6 mM Mn^{2+}, and 90 min incubation time of Mn^{2+} were set as optimal conditions.

Analytical Performance. To verify the as-designed ratiometric biosensor for quantitative detection, various concentrations of miRNA-21 were then measured. As evident from Figure 7A, the DPV response was changed gradually when the concentration of miRNA-21 was increased within 0.5 fM−5 nM. With the increase of the amount of miRNA-21, the signal response of UiO-66-SP was decreased gradually. However, the response of $[Fe(CN)_6]^{3-/4-}$-IR was increased gradually. Thus, the $I_{[Fe(CN)6]^{3-/4-}\text{-IR}}/I_{\text{UiO-66-SP}}$ ratio value was increased when the concentration of miRNA-21 increased (Figure 7B). Figure 7C shows the linear relationship between the logarithm of miRNA-21 concentration with the ratio value.

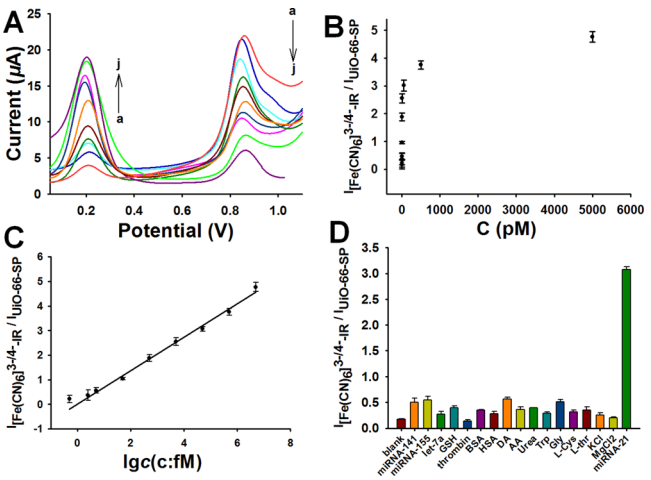

Figure 7. (A) DPV current response of the sensor to miRNA-21 at different concentrations ((a) 0, (b) 0.5 fM, (c) 2.5 fM, (d) 5 fM, (e) 0.05 pM, (f) 0.5 pM, (g) 5 pM, (h) 0.05 nM, (i) 0.5 nM, (j) 5 nM); (B) the ratio value was increased with the enhancement of target concentration; (C) calibration curves for miRNA-21 detection; (D) selectivity of the sensor.

The regression equation is $I_{[Fe(CN)6]^{3-/4-}\text{-IR}}/I_{\text{UiO-66-SP}} = 0.6522 \lg C + 0.1413$. Also, according to the expression of $3\sigma/S$, the LOD obtained was 0.17 fM. The performance of the as-designed sensor is compared with other sensing systems and summarized in Table S2.[41−47] The results show that the sensor designed in this paper is better in terms of linear range and detection limit.

The interfering substances including miRNA-141, let-7a, miRNA-155, GSH, thrombin, BSA, AA, urea, Trp, Gly, L-Cys, L-thr, K^+, and Mg^{2+} were selected to further study the selectivity of the constructed biosensor toward miRNA-21. Although a high concentration of electroactive molecules AA and DA (5 M) could directly detect the current response, the signal can be detected at +0.3 V (AA) and +0.6 V (DA). These signal is different from the signal response of UiO-66 at +0.9 V (Figure S2). When the concentration of AA and DA was decreased (0.5 nM), the current signal cannot be detected. Moreover, our proposed method is based on the two signal input; thus, these factors can be ignored. As displayed in Figure 7D, even though the concentration of the interfering substance (0.5 nM) was 10 times higher than the target (0.05 nM), only the target could obtain the highest ratio value. The results showed that the constructed sensor owned strong selectivity for miRNA-21.

Reproducibility and Stability of Biosensor. To study the detection repeatability of the constructed strategy, 10 GCEs were selected, and then, 20 tests were carried out under the same conditions. The results showed a significant change for the nonproportional strategy, with a mean current of 2.30 μA (Figure 8A) and a relative standard deviation (RSD) of 51.4%. This variation could prominently be decreased in our designed strategy, and the average current ratio of the 20 tests was 3.09, and the RSD was 4.35% (Figure 8B). The results showed that the ratiometric analysis afforded acceptable repeatability (Figure 8C). The ratiometric dual-signal strategy could reduce the interference of environmental factors and basic electrode characteristics, so the designed ratiometric electrochemical strategy for miRNA-21 analysis had an excellent reproducibility.

https://doi.org/10.1021/acs.langmuir.2c00932
Langmuir 2022, 38, 11828−11836

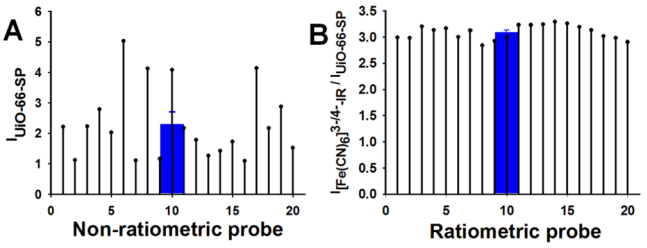

C

	$I_{Zr\text{-}MOFs}$	$I_{[Fe(CN)6]^{3-/4-}\text{-}rP}$ / $I_{Zr\text{-}MOFs\text{-}sp}$	RSD
Non-ratiometric method	2.31[a] ± 0.92[b]		51.4%
Ratiometric method		3.09[a] ± 0.12[b]	4.35%

Figure 8. (A) Current intensity of the nonproportional sensor. (B) Current ratio value of the ratiometric sensor. (The black line represents the ratio value of 20 tests. The blue histograms represent average values of 20 measurements and the RSD.) (C) Comparison of proportional and nonproportional sensors. a is the average value, and b is the standard deviation.

Detection of miRNA-21 in Serum Samples. To investigate the proposed ratio biosensor for real sample applications, miRNA-21 in human serum samples by standard addition methods was tested, and recoveries were obtained. Blood samples were centrifuged (1200 r/min) for 3 min to obtain a serum sample, which was received from Hospital of Yunnan Normal University (Kunming, China). After being diluted 100-fold with PBS buffer, the serum samples were mixed with miRNA with the final concentrations of 0.05, 0.8, and 50.0 pM. The experimental procedure was consistent with the sensor preparation. Table S3 depicted the results of the detection of miRNA-21 (0.05, 0.8, and 50.0 pM) in three serum samples. As can be seen from the table, the recoveries of miRNA-21 ranged from 95.66 to 104.4%, and the RSD ranged from 0.93 to 1.81%, illustrating that this designed ratiometric biosensor could be utilized to detect miRNA-21 in real actual samples.

CONCLUSIONS

An enzyme-free DNA-walker-based ratiometric electrochemical biosensor in combination with a Zr MOF signal tag (UiO-66) to detect miRNA was presented. Our report demonstrates using UiO-66 first as an electrochemical signal tag for a biosensor. its current signal can be detected at +0.9 V in neutral conditions. With UiO-66 as a signal probe, the signal is strong and stable. Unlike the previous ratiometric electrochemical biosensor, in which electrolyte solution $K_3Fe(CN)_4$/$K_4Fe(CN)_6$ was the reference probe, it is cheap, stable, and can be used without modification. In the presence of target, the current intensity of UiO-66 at +0.9 V was decreased. Meanwhile, the current signal of electrolyte solution as a reference at +0.2 V was increased due to the enhancement of electrode conductivity. Thus, a ratiometric electrochemical biosensor in combination with UiO-66 signal tags to detect miRNA was developed. A DNA tetrahedron with a well-controlled orientation characteristic can reduce the local overcrowding effect to increase the efficiency of a DNA walker. Taking advantage of UiO-66 signal tags to obtain a stable signal and NTH-based-DNA walker signal amplification, this ratiometric biosensor shows ultrasensitivity to miRNA-21 with an LOD of 170 aM. It can also provide more accurate signals, in which environmental factors and basic electrode characteristics were eliminated. As expected, it is hoped that the approach could be ideally suitable for biomaker analysis in clinical detection.

ASSOCIATED CONTENT

Supporting Information

The Supporting Information is available free of charge at https://pubs.acs.org/doi/10.1021/acs.langmuir.2c00932.

DNA sequences used in this experiment (Table S1); feasibility of our experiment (Figure S1); current response of AA and DA on the GCE electrode (Figure S2); comparison of different methods for miRNA detection (Table S2); recovery of miRNA in human serum samples (Table S3) (PDF)

AUTHOR INFORMATION

Corresponding Authors

Rong Hu − *College of Chemistry and Chemical Engineering, Yunnan Normal University, Kunming, Yunnan 650500, P.R. China*; Phone: 86-871-65941087; Email: hudierong_168@163.com

Yun-Hui Yang − *College of Chemistry and Chemical Engineering, Yunnan Normal University, Kunming, Yunnan 650500, P.R. China*; orcid.org/0000-0001-9235-7274; Phone: 86-871-65941087; Email: yyhui2002@aliyun.com

Authors

Fa-Ting Xie − *College of Chemistry and Chemical Engineering, Yunnan Normal University, Kunming, Yunnan 650500, P.R. China*

Yu-Long Li − *College of Chemistry and Chemical Engineering, Yunnan Normal University, Kunming, Yunnan 650500, P.R. China*

Tong Yang − *College of Chemistry and Chemical Engineering, Yunnan Normal University, Kunming, Yunnan 650500, P.R. China*; orcid.org/0000-0003-4438-2568

Complete contact information is available at: https://pubs.acs.org/10.1021/acs.langmuir.2c00932

Author Contributions

F.-T.X. and Y.-L.L. made equal contributions to this research

Notes

The authors declare no competing financial interest.

ACKNOWLEDGMENTS

This work was supported by the National Natural Science Foundation of China (No. 21864026 and 21605130) and the Scientific Research Innovation Fund of Yunnan Normal University.

REFERENCES

(1) Zhao, B.; Qi, L.; Tai, W.; Zhao, M.; Chen, X.; Yu, L.; Shi, J.; Wang, X.; Lin, J.-M.; Hu, Q. Paper-based flow sensor for the detection of hyaluronidase via an enzyme hydrolysis-induced viscosity change in a polymer solution. *Anal. Chem.* **2022**, *94*, 4643.

(2) Zhu, C. X.; Liu, D.; Li, Y. Y.; Shen, X. L.; Li, L. B.; Liu, Y.; You, T. Y. Ratiometric electrochemical, electrochemiluminescent, and photoelectrochemical strategies for environmental contaminant detection. *Curr. Opin. Electrochem.* **2019**, *17*, 47−55.

(3) Labib, M.; Sargent, E. H.; Kelley, S. O. Electrochemical methods for the analysis of clinically relevant biomolecules. *Chem. Rev.* **2016**, *116*, 9001−9090.
(4) Cao, Y.; Liu, J. J.; Zou, L. N.; Ye, B. X.; Li, G. P. Ratiometric fluorescence sensing of glutathione by using the oxidase-mimicking activity of MnO_2 nanosheet. *Anal. Chim. Acta* **2021**, *1145*, 46−51.
(5) Zhu, C. X.; Liu, D.; Li, Y. Y.; Shen, X. L.; Li, L. B.; Liu, Y.; You, T. Y. Ratiometric electrochemical, electrochemiluminescent, and photoelectrochemical strategies for environmental contaminant detection. *Curr. Opin. Electrochem.* **2019**, *17*, 47−55.
(6) Ahmadi, A.; Danesh, N. M.; Ramezani, M.; Alibolandi, M.; Lavaee, P.; Emrani, A. S.; Abnous, K.; Taghdisi, S. M. A rapid and simple ratiometric fluorescent sensor for patulin detection based on a stabilized DNA duplex probe containing less amount of aptamer-involved base pairs. *Talanta* **2019**, *204*, 641−646.
(7) Zhao, Y.; Yang, Y.; Cui, L.; Zheng, F.; Song, Q. Electroactive Au@Ag nanoparticles driven electrochemical sensor for endogenous H_2S detection. *Biosens. Bioelectron.* **2018**, *117*, 53−59.
(8) Zhang, Y.; Nie, J. T.; Wei, H. Y.; Xu, H. T.; Wang, Q.; Cong, Y. Q.; Tao, J. Q.; Zhang, Y.; Chu, L. L.; Zhou, Y.; Wu, X. Y. Electrochemical detection of nitrite ions using Ag/Cu/MWNT nanoclusters electrodeposited on a glassy carbon electrode. *Sens. Actuator B-Chem.* **2018**, *258*, 1107−1116.
(9) Wan, Y.; Zhou, Y.; Poudineh, M.; Safaei, T. S.; Mohamadi, R. M.; Sargent, E. H.; Kelley, S. O. Highly specific electrochemical analysis of cancer cells using multi-nanoparticle labeling. *Angew. Chem., Int. Ed.* **2014**, *53*, 13145−13149.
(10) Chen, Y.; Ahn, S.; Mian, M. R.; Wang, X.; Ma, Q.; Son, F. A.; Yang, L.; Ma, K.; Zhang, X.; Notestein, J. M.; Farha, O. K. Modulating chemical environments of metal-organic framework-supported molybdenum(VI) catalysts for insights into the structure-activity relationship in cyclohexene epoxidation. *J. Am. Chem. Soc.* **2022**, *144*, 3554−3563.
(11) Liu, J. L.; Ma, Y. C.; Yang, T.; Hu, R.; Yang, Y. H. A single nucleotide polymorphism electrochemical sensor based on DNA-functionalized Cd-MOFs-74 as cascade signal amplification probes. *Microchim. Acta* **2021**, *188*, 266.
(12) Hu, R.; Zhang, X.; Chi, K. N.; Yang, T.; Yang, Y. H. Bifunctional MOFs-based ratiometric electrochemical sensor for multiplex heavy metal ions. *ACS Appl. Mater. Interfaces* **2020**, *12*, 30770−30778.
(13) Liu, T. Z.; Hu, R.; Zhang, X.; Zhang, K. L.; Liu, Y.; Zhang, X. B.; Bai, R. Y.; Li, D. L.; Yang, Y. H. Metal-organic frameworks nanomaterials as novel signal probes for electron transfer mediated ultrasensitive electrochemical immunoassay. *Anal. Chem.* **2016**, *88*, 12516−12523.
(14) Carrington, E. J.; McAnally, C. A.; Fletcher, A. J.; Thompson, S. P.; Warren, M.; Brammer, L. Solvent-switchable continuous-breathing behaviour in a diamondoid metal-organic framework and its influence on CO_2 versus CH_4 selectivity. *Nat. Chem.* **2017**, *9*, 882−889.
(15) Liu, Y.; Hou, W. J.; Xia, L.; Cui, C.; Wan, S.; Jiang, Y.; Yang, Y.; Wu, Q.; Qiu, L. P.; Tan, W. H. Zr MOF nanoparticles as quenchers to conjugate DNA aptamers for target-induced bioimaging and photodynamic therapy. *Chem. Sci.* **2018**, *9*, 7505−7509.
(16) Wang, X. L.; Rehman, A.; Kong, R. M.; Cheng, Y. Y.; Tian, X. X.; Liang, M. S.; Zhang, L. D.; Xia, L. A.; Qu, F. G. Naphthalimide derivative-functionalized metal-organic framework for highly sensitive and selective determination of aldehyde by space confinement-induced sensitivity enhancement effect. *Anal. Chem.* **2021**, *93*, 8219−8227.
(17) Zhou, N.; Su, F. F.; Guo, C. P.; He, L. H.; Jia, Z. K.; Wang, M. H.; Jia, Q. J.; Zhang, Z. H.; Lu, S. Y. Two-dimensional oriented growth of Zn-MOF-on-Zr-MOF architecture: A highly sensitive and selective platform for detecting cancer markers. *Biosens. Bioelectron.* **2019**, *123*, 51−58.
(18) Chang, J. F.; Wang, X.; Wang, J.; Li, H. Y.; Li, F. Nucleic acid-functionalized metal-organic framework-based homogeneous electrochemical biosensor for simultaneous detection of multiple tumor biomarkers. *Anal. Chem.* **2019**, *91*, 3604−3610.
(19) Yan, T. T.; Zhu, L. Y.; Ju, H. X.; Lei, J. P. DNA-walker-induced allosteric switch for tandem signal amplification with palladium nanoparticles/metal-organic framework tags in electrochemical biosensing. *Anal. Chem.* **2018**, *90*, 14493−14499.
(20) Galardi, A.; Colletti, M.; Di Paolo, V.; Vitullo, P.; Antonetti, L.; Russo, I.; Di Giannatale, A. Exosomal MiRNAs in pediatric cancers. *Int. J. Mol. Sci.* **2019**, *20*, 4600.
(21) Yoshida, K.; Yokoi, A.; Yamamoto, Y.; Kajiyama, H. ChrXq27.3 miRNA cluster functions in cancer development. *J. Exp. Clin. Cancer Res.* **2021**, *40*, 112.
(22) Tinel, C.; Lamarthee, B.; Anglicheau, D. MicroRNAs: small molecules, big effects. *Curr. Opin. Organ Transpl.* **2021**, *26*, 10−16.
(23) Hull, M. L.; Nisenblat, V. Tissue and circulating microRNA influence reproductive function in endometrial disease. *Reprod. Biomed. Online* **2013**, *27*, 515−529.
(24) Plotkin, L. I.; Wallace, J. M. MicroRNAs and osteocytes. *Bone* **2021**, *150*, 115994.
(25) Kandettu, A.; Radhakrishnan, R.; Chakrabarty, S.; Sriharikrishnaa, S.; Kabekkodu, S. P. The emerging role of miRNA clusters in breast cancer progression. *Biochim. Biophys. Acta-Rev. Cancer* **2020**, *1874*, 188413.
(26) Rupaimoole, R.; Calin, G. A.; Lopez-Berestein, G.; Sood, A. K. miRNA deregulation in cancer cells and the tumor microenvironment. *Cancer Discovery* **2016**, *6*, 235−246.
(27) Li, Y.; Du, S. S.; Chai, Z. L.; He, J. L. A new Pb^{2+}-specific DNAzyme by revisiting the catalytic core of 10−23 DNAzyme. *Bioorg. Med. Chem.* **2020**, *28*, 115796.
(28) Kilic, T.; Erdem, A.; Ozsoz, M.; Carrara, S. microRNA biosensors: Opportunities and challenges among conventional and commercially available techniques. *Biosens. Bioelectron.* **2018**, *99*, 525−546.
(29) Cheng, X.; Bao, Y.; Liang, S.; Li, B.; Liu, Y.; Wu, H.; Ma, X.; Chu, Y.; Shao, Y.; Meng, Q.; Zhou, G.; Song, Q.; Zou, B. Flap Endonuclease 1-assisted DNA walkers for sensitively and specifically sensing ctDNAs. *Anal. Chem.* **2021**, *93*, 9593−9601.
(30) Wang, L.; Liu, P.; Liu, Z.; Zhao, K.; Ye, S.; Liang, G.; Zhu, J. Simple tripedal DNA walker prepared by target-triggered catalytic hairpin assembly for ultrasensitive electrochemiluminescence detection of MicroRNA. *ACS Sensors* **2020**, *5*, 3584−3590.
(31) Li, Z. H.; Zhao, B.; Wang, D. F.; Wen, Y. L.; Liu, G.; Dong, H. Q.; Song, S. P.; Fan, C. H. DNA nanostructure-based universal microarray platform for high-efficiency multiplex bioanalysis in biofluids. *ACS Appl. Mater. Interfaces* **2014**, *6*, 17944−17953.
(32) Lin, Y.; Jia, J. P.; Yang, R.; Chen, D. Z.; Wang, J.; Luo, F.; Guo, L. H.; Qiu, B.; Lin, Z. Y. Ratiometric immunosensor for GP73 detection based on the ratios of electrochemiluminescence and electrochemical signal Using DNA tetrahedral nanostructure as the carrier of stable reference signal. *Anal. Chem.* **2019**, *91*, 3717−3724.
(33) Lin, M. H.; Wang, J. J.; Zhou, G. B.; Wang, J. B.; Wu, N.; Lu, J. X.; Gao, J. M.; Chen, X. Q.; Shi, J. Y.; Zuo, X. L.; Fan, C. H. Programmable engineering of a biosensing interface with tetrahedral DNA nanostructures for ultrasensitive DNA detection. *Angew. Chem., Int. Ed.* **2015**, *54*, 2151−2155.
(34) Li, J.; Fan, C. H.; Pei, H.; Shi, J. Y.; Huang, Q. Smart drug delivery nanocarriers with self-assembled DNA nanostructures. *Adv. Mater.* **2013**, *25*, 4386−4396.
(35) Huang, M. F.; Kuo, Y. C.; Huang, C. C.; Chang, H. T. Separation of long double-stranded DNA by nanoparticle-filled capillary electrophoresis. *Anal. Chem.* **2004**, *76*, 192−196.
(36) Luo, B. C.; Yuan, L. Y.; Chai, Z. F.; Shi, W. Q.; Tang, Q. U(VI) capture from aqueous solution by highly porous and stable MOFs: UiO-66 and its amine derivative. *J. Radioanal. Nucl. Chem.* **2016**, *307*, 269−276.
(37) Abid, H. R.; Shang, J.; Ang, H. M.; Wang, S. B. Amino-functionalized Zr-MOF nanoparticles for adsorption of CO_2 and CH_4. *Int. J. Smart Nano Mater.* **2013**, *4*, 72−82.
(38) Petraki, F.; Papaefthimiou, V.; Kennou, S. The electronic structure of Ni-phthalocyanine/metal interfaces studied by X-ray and

https://doi.org/10.1021/acs.langmuir.2c00932
Langmuir 2022, 38, 11828−11836

ultraviolet photoelectron spectroscopy. *Org. Electron.* **2007**, *8*, 522−528.
(39) Erdogan, N. H.; Kara, K.; Ozdamar, H.; Esen, R.; Kavak, H. Effect of the oxidation temperature on microstructure and conductivity of ZnxNy thin films and their conversion into p-type ZnO: N films. *Appl. Surf. Sci.* **2013**, *271*, 70−76.
(40) Song, D. D.; Jiang, X. Y.; Li, Y. S.; Lu, X.; Luan, S. R.; Wang, Y. Z.; Li, Y.; Gao, F. M. Metal-organic frameworks-derived MnO_2/Mn_3O_4 microcuboids with hierarchically ordered nanosheets and Ti_3C_2 MXene/Au NPs composites for electrochemical pesticide detection. *J. Hazard. Mater.* **2019**, *373*, 367−376.
(41) Luo, L. P.; Wang, L. L.; Zeng, L. P.; Wang, Y. R.; Weng, Y. P.; Liao, Y. J.; Chen, T. T.; Xia, Y. K.; Zhang, J.; Chen, J. H. A ratiometric electrochemical DNA biosensor for detection of exosomal MicroRNA. *Talanta* **2020**, *207*, 120298.
(42) Xue, C.; Zhang, S.; Li, C.; Yu, X.; Ouyang, C.; Lu, Y.; Wu, Z. Y-shaped backbone-rigidified triangular DNA scaffold-directed stepwise movement of a DNAzyme walker for sensitive MicroRNA imaging within living cells. *Anal. Chem.* **2019**, *91*, 15678−15685.
(43) Wu, T.; Yang, Y.; Cao, Y.; Song, Y.; Xu, L.; Zhang, X.; Wang, S. Bioinspired DNA-inorganic hybrid nanoflowers combined with a personal glucose meter for onsite detection of miRNA. *ACS Appl. Mater. Interfaces* **2018**, *10*, 42050−42057.
(44) Zhong, W.; Wu, J.; Huang, Y.; Xing, C.; Lu, C. Target-activated, light-actuated three-dimensional DNA walker nanomachine for amplified miRNA Detection. *Langmuir* **2022**, *38*, 1151−1157.
(45) Su, S.; Sun, Q.; Ma, J.; Zhu, D.; Wang, F.; Chao, J.; Fan, C.; Li, Q.; Wang, L. Ultrasensitive analysis of microRNAs with gold nanoparticle-decorated molybdenum disulfide nanohybrid-based multilayer nanoprobes. *Chem. Commun.* **2020**, *56*, 9012−9015.
(46) Fang, C. S.; Kim, K.; Yu, B.; Jon, S.; Kim, M.; Yang, H. Ultrasensitive electrochemical detection of miRNA-21 using a zinc finger protein specific to DNA-RNA hybrids. *Anal. Chem.* **2017**, *89*, 2024−2031.
(47) Chu, Y.; Wu, R.; Fan, G.; Deng, A.; Zhu, J. Enzyme-Free photoelectrochemical biosensor based on the Co-sensitization effect coupled with dual cascade toehold-mediated strand displacement amplification for the sensitive detection of MicroRNA-21. *ACS Sustainable Chem. Eng.* **2018**, *6*, 11633−11641.

https://doi.org/10.1021/acs.langmuir.2c00932
Langmuir 2022, 38, 11828−11836